Uncovering Low-Dimensional Manifolds of Neural Dynamics for Motor-Imagery Based Stroke Rehabilitation: An EEG-Based Brain–Computer Interface Study

Tao Liu, Ziwei Wang, Sadia Shakil, and Raymond Kai-Yu Tong, *Senior Member, IEEE*

***Abstract*— Stroke rehabilitation aims to repair neural circuits and dynamics through the remapping of neuronal functions. However, there is currently a gap in understanding the alteration of neural population dynamics-the fundamental computational unit driving functions-under clinical settings. In this study, we introduced a novel method to identify stable low-dimensional structures of neural population dynamics in stroke patients during motor tasks. Using whole-brain EEG recordings from chronic stroke patients performing motor imagery (MI) tasks before and after brain-computer interface (BCI) training, as well as a public EEG dataset of acute stroke patients performing MI tasks, we projected EEG signals from sensor space to voxel space via source localization (eLORETA), simulating neural population activity in regions of interest. By applying dimensionality reduction, we successfully obtained low-dimensional neural manifolds to represent neural population dynamics. Our analysis revealed three key findings: (1) For right-handed patients, task-related low-dimensional dynamics in the related brain regions remain stable across subjects, with their features holding potential as biomarkers for stroke rehabilitation; (2) BCI training promotes global and sustained restoration of neural population dynamics; (3) EEG theta-band oscillations show strong correlation with these dynamics, highlighting their macroscopic nature. This study proposes a new, simple, and powerful tool for comprehension and validation of stroke rehabilitation mechanisms confirming the effectiveness of BCI training in restoring neural dynamics.**

Received 26 February 2025; revised 15 July 2025; accepted 17 August 2025. Date of publication 20 August 2025; date of current version 27 August 2025. This work was supported in part by The Chinese University of Hong Kong under Direct Grant 4055211; in part by the General Research Fund through the Research Grant Council of Hong Kong under Grant CUHK14216622; and in part by the China Scholarship Council Program under Grant 202408060125. *(Corresponding authors: Sadia Shakil; Raymond Kai-Yu Tong.)*

This work involved human subjects or animals in its research. Approval of all ethical and experimental procedures and protocols was granted by Chinese University of Hong Kong Rehabilitation Laboratories under Application No. NCT02323061.

Tao Liu is with the Nuffield Department of Clinical Neurosciences, University of Oxford, OX3 9DU Oxford, U.K. (e-mail: tao.liu@ndcn.ox.ac.uk).

Ziwei Wang is with the Department of Biomedical Engineering, The Hong Kong Polytechnic University, Hong Kong (e-mail: jay0516.wang@connect.polyu.hk).

Sadia Shakil and Raymond Kai-Yu Tong are with the Department of Biomedical Engineering, The Chinese University of Hong Kong, Hong Kong (e-mail: sadiashakil@cuhk.edu.hk; kytong@cuhk.edu.hk).

This article has supplementary downloadable material available at https://doi.org/10.1109/TNSRE.2025.3600824, provided by the authors.

Digital Object Identifier 10.1109/TNSRE.2025.3600824

***Index Terms*— EEG, neural population dynamics, motor imagery, brain-computer interface, stroke rehabilitation.**

I. Introduction

POST-STROKE recovery involves improving functional impairments over time through functional remapping along with redundant and segregation mechanisms in the brain, where surviving neurons compensate for lost functions through both local circuit adaptation and interregional communication [1], [2], [3], [4]. However, traditional neuroimaging approaches focusing on regional activation magnitude or coarse connectivity patterns fail to capture the spatiotemporal dynamics of neuronal population activity - the fundamental computational unit driving functions [5], [6]. Recent advances in neural population dynamics reveal that stroke-induced circuit reorganization is not only reflected in the reconstruction of functional connectivity, but also manifests as reconfiguration of the spatiotemporal activation patterns of neural populations [7]. This critical gap in understanding the mesoscopic neural dynamics reflecting recovery requires new analytical frameworks to describe how existing therapeutic interventions reshape population-level neural dynamics in damaged circuits.

Currently, rehabilitation involving motor-imagery-based brain-computer interface (MI-BCI) training is regarded as an effective long-term treatment for stroke-related movement disorders [8]. Several studies have demonstrated that MI-BCI training can enhance motor skills [9], [10], [11] and restore function by activating broader brain regions and reestablishing neural pathways in stroke patients [8], [12]. For example, task-related brain functional network reconstruction [13], motor cortex functional connectivity modulation [14], and hemispheric asymmetry reduction [15] have been observed on patients following MI-BCI training.

The above studies revealed the consistency of neural circuit reconstruction during stroke rehabilitation, which may correspond to consistent changes in the temporal patterns of behavior-related neuronal population's activity throughout recovery. Specifically, certain neurons in a specific brain area exhibit spatiotemporal activation during movement, which can be defined as a distinct neural mode. The activity of the neural population can be described as a combination of multiple neural modes, thereby encoding the population

dynamics in the neural modes space [5]. Recent studies have shown that movement-related neural population dynamics can be represented as specific low-dimensional neural manifolds in the neural mode space, which remain stable across tasks, time, and subjects [16], [17], [18]. Stroke disrupts movement-related population dynamics and affects the activity of regions in the circuit, while stroke recovery reflects the normalization of the neural population activity and circuit function [19], [20], [21]. Therefore, the low-dimensional manifold of movement-related neural population activity may offer insights into the consistent changes in neural population dynamics during stroke rehabilitation.

While low-dimensional neural manifolds have been observed in healthy individuals during motor imagery tasks [22], there is no direct evidence of this phenomenon in stroke patients. Additionally, most previous studies have relied on invasive brain recordings, whereas MI-BCI rehabilitation typically uses non-invasive EEG recordings. As a result, there is limited research demonstrating the applicability of low-dimensional neural manifolds in MI-BCI rehabilitation using EEG data.

In this paper, we hypothesize that stable low-dimensional neural population dynamics exist in task-related brain regions of stroke patients performing motor imagery task, with their structures evolving consistently with stroke rehabilitation. To this end, we developed an MI-BCI rehabilitation paradigm and conducted experiments with several chronic stroke patients. To connect non-invasive EEG recordings and neural population activities, we introduce source localization to project EEG signals from sensor space to voxel space, obtaining source activities to simulate neural population activities. To remove redundant information and combine neuronal activities (voxels activities) into neural modes, principal component analysis (PCA) was employed to extract low-dimensional dynamics. Fig. 2. shows the outline of our research. Our findings indicate that the task-related low-dimensional neural manifold derived from EEG remains stable across subjects. Additionally, the structure of the manifolds as well as neural modes reflect the progress of stroke recovery. The strong correlation between the low-dimensional neural manifolds and the low-frequency EEG oscillations further supports its biological significance. All relevant codes and example data are available on https://github.com/JayWIIOZ/EEG-Neural-Manifolds.

Our contributions are four-folds:

- Confirmation of the existence of stable low-dimensional neural population dynamics in stroke patients performing motor imagery tasks.
- Development of an effective EEG-based method for extracting stable, task-related low-dimensional neural manifolds.
- Reflection of the stroke rehabilitation process in patients through consistent neural manifold structure.
- Estimation of correlation between neural manifolds and EEG oscillations, providing insight into the underlying nature of these manifolds.

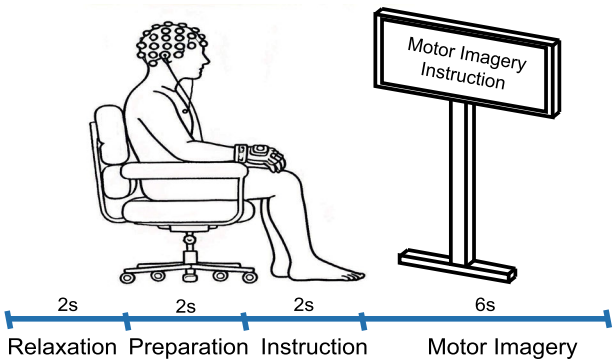

Fig. 1. Schematic diagram of stroke patient performing BCI training following motor imagery instruction. The bottom line shows the process of the task.

II. Materials and Methodology

A. Materials

1) Chronic Stroke Datasets: Seven chronic stroke patients (6 males, 1 female, all right-handed) with unilateral hemispheric impairment participated in this study. Each patient underwent 20 sessions of brain-computer-interface guided, robot-assisted upper-limb training over 5 to 7 weeks, with the motor functions of the paretic upper limbs assessed by Fugl-Meyer Assessment for upper extremity (FMA) [15]. Before and after training, participants completed a motor imagery task following a predefined paradigm, with real-time EEG-fMRI recordings. 2 MI sessions and 1 resting session are recorded for both pre- and post- training, with each MI session containing 13-14 trials, each resting session containing around 200 trials. Each trial of resting session only lasts for 2 s. The MI task involved alternating between imagining 'hand grasp' and 'hand open' movements based on visual instructions. The task flow is shown in Fig. 1. A white cross helping the subject concentrate and text instruction of 'grasp' or 'open' would be shown on screen during the preparation and instruction phases, respectively. Patients were required to perform the instructed imagery in the following 6 s [23]. Significant improvement in FMA scores has been observed after BCI training (Wilcoxon signed rank test, $p = 3.13 \times 10^{-2}$<0.05, $cohen's\ d = 0.47$, $power = 0.18$, Supplementary Table 1), manifesting the effectiveness of BCI training in stroke rehabilitation. One MI session was discarded for both before and after training due to data lost and great noise. More details on patients and BCI training are provided in Supplementary Table 1 and Section III of the Supplementary Material.

EEG data was recorded using the Neuroscan system (SynAmps2, Neuroscan Inc., Herndon, USA) with 64 Ag/AgCl electrodes placed according to the standard 10-20 system. Two additional electrocardiogram (ECG) electrodes were placed in the left lower chest and near the upper midline, and one electrooculogram (EOG) electrode was placed below the right eye. The central point between Cz and CPz was used as the reference, with AFz as the ground. Electrode impedance was maintained below 5 kOhms. Data were sampled at 1000 Hz, with a 0.1-256 Hz bandpass Butterworth filter applied during offline processing.

In addition, structural magnetic resonance (sMRI) scans were collected from all subjects before and after BCI

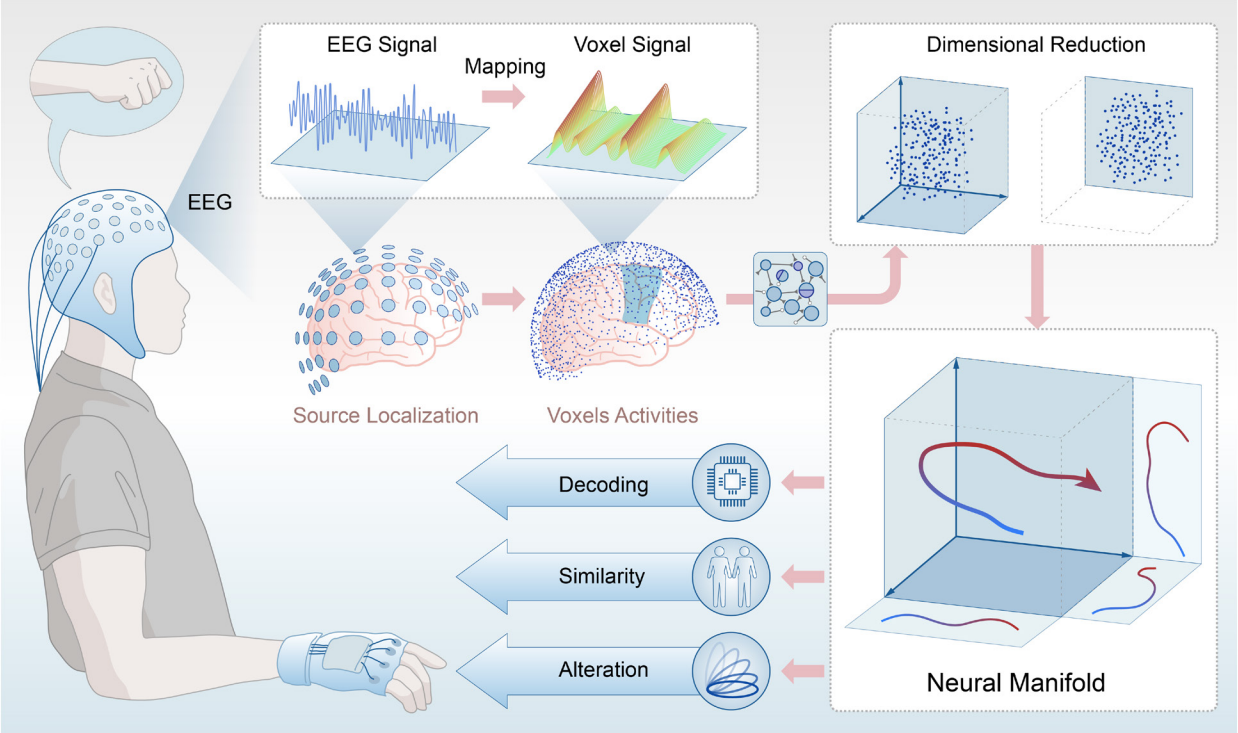

Fig. 2. Illustration of the process of uncovering low-dimensional neural manifolds based on EEG. Real-time EEG was recorded during patients performing MI task. Then, Source localization using eLORETA was applied to map EEG signals from electrode space to voxel space. Subsequently, dimensional reduction, which is PCA in this study, was applied to voxel activities of ROIs to obtain low-dimensional neural manifolds which would be used for exploring decoding performance, cross-subject and cross-session similarity as well as alteration induced by rehabilitation.

training. T1-weighted MRI images were acquired using a 3T Philips MR scanner (Achieva TX, Philips Medical Systems, Best, Netherlands) with an 8-channel head coil and a T1-TFE sequence. The imaging parameters were: TR/TE = 7.47/3.45 ms, flip angle = 8°, 308 slices, and voxel size = $0.6 \times 1.042 \times 1.042$ mm^3. This study focused on EEG recordings and structural MRI, for details of fMRI recordings, please refer to [15] and [23].

This study was approved by the Joint Chinese University of Hong Kong-New Territories East Cluster Clinical Research Ethics Committee. All subjects gave written consent before the intervention and underwent the experiments in the Chinese University of Hong Kong rehabilitation labs. This study was registered at https://clinicaltrials.gov (NCT02323061).

2) Acute Stroke Dataset: A publicly available EEG motor imagery dataset for brain-computer interface in acute stroke patients was used for validation [24]. 30 acute stroke subjects (23 males, 7 females, 14 left hemiplegia, 16 right hemiplegia) were screened in this study. The neurological status and severity of stroke in acute stroke patients were assessed by the National Institute of Health Stroke Scale (NIHSS) score. The MI experiment consisted of 40 trials alternating between left- and right-hand motor imagery, each lasting 8 seconds and divided into three stages: instruction, motor imagery (MI), and break. Subjects were first prompted to imagine grasping a spherical object with the left or right hand for 2s, with the following image of the action while watching a video of the motion for 4s before a break [24].

The EEG data were recorded by a wireless multichannel EEG acquisition system (ZhenTec NT1, Xi'an ZhenTec Intelligence Technology Co., Ltd., China), with 29 Ag/AgCl semi-dry EEG electrodes (3% NaCl solution) and 2 EOG electrodes positioned according to the 10-10 system, with CPz and FPz as the reference and ground, respectively. The sampling rate was 500 Hz, and acquisition impedance was $\leq$ 20 kOhms. More detailed information can be found in [24].

B. Preprocessing

EEG signal preprocessing for chronic stroke dataset was primarily conducted using EEGLAB [25], [26] and Fieldtrip Toolbox [27]. First, a principal component analysis (PCA)-based optimal basis set (OBS) algorithm [28] was applied to remove gradient artifacts caused by fMRI, with the EEG signals and fMRI volume triggers as input. Next, an R-peak detection algorithm [29] was employed to eliminate the ECG artifacts. The signals were then band-pass filtered between 1 and 50 Hz to isolate the frequency band of interest and notch filtered at 50 Hz to remove line noise. Damaged channels were removed and interpolated, followed by common average re-referencing. The signals were segmented into 12-second epochs to capture the entire motor imagery task trial. Finally, adaptive mixture independent component analysis (AMICA) [30] was used to remove the EOG/EMG-related components.

Structural and functional MRI preprocessing were performed using the Data Processing Assistant for Resting-State fMRI (DPARSF) toolbox [31], following the default

procedure. This included removing first 10 volumes, nuisance covariates regression, head motion correction (Friston 24 parameters), scrubbing, realignment, detrending, band-pass filtering (0.01-0.1 Hz), spatial normalization to the Montreal Neurological Institute (MNI) template, reslicing to $2 \times 2 \times 2$ mm^3 voxels and smoothing with a 6 mm full-width at half-maximum (FWHM) Gaussian kernel.

In terms of the acute stroke dataset, similar preprocessing was conducted but without the removal of gradient artifacts. The signals were segmented into 8-second epochs for analysis.

C. Source Localization

To estimate cortical-level neural population activity from scalp EEG recordings, we employed a distributed source model, which divides the cortical volume into thousands of dipoles and assumes continuous current dipole distributions across cortical voxels. By solving the underdetermined inverse problem through regularized optimization, we will be able to obtain the optimal estimation of dipole activities [32]. The sensor-to-source projection follows the linear forward model:

$$\Phi = \mathbf{K}\mathbf{J} + \epsilon \tag{1}$$

where Φ refers to the EEG electrode signals, $\mathbf{K}$ the lead field matrix, $\mathbf{J}$ the cortical source currents and ϵ the measurement noise.

The pre-processed EEG and sMRI were involved for EEG source localization using eLORETA [33] to project EEG signal from electrode space to voxel space. The forward model was built with a 10 mm grid resolution. Individual head model was constructed for each subject based on the sMRI image utilizing openMEEG [34]. A public head model template was used for the source localization for the public acute stroke dataset. After source localization, the obtained dipoles, which represent the estimated source of brain activities, were interpolated into the automated anatomical labeling atlas (AAL, 2 mm resolution) [35]. This resulted in $91 \times 109 \times 91$ 2-mm voxels in the brain. Eight regions of interest (ROIs) were selected based on the AAL atlas. These brain regions have been previously implicated in the process of motor imagery, and changes in their functional connectivity may reflect stroke recovery [23], [36]. The voxel activities within these regions were used to simulate neural population activity. The coordinates, abbreviations and voxel number of these ROIs corresponding to the AAL atlas used for subsequent analysis are shown in Supplementary Table 2.

D. Low-Dimensional Neural Manifolds

To characterize the dynamics of neural population activity over time during the motor imagery task, we divided the voxel time series into non-overlapping 30 ms time windows and the samples within each window were averaged to represent real-time voxel activity dynamics. The smoothed time series was then treated as the representation of temporal dynamics of voxel activity. The resulting trials $\times$ voxels $\times$ windows matrix (N $\times$ V $\times$ T) served as input for further analysis. PCA model was fitted with the concatenated matrix of input along the trials axis (V $\times$ N*T) and used to transform the V $\times$ T matrix of each trial. This process can be described as

$$\bar{\mathbf{X}}_{n,t} = \frac{1}{S}\sum_{s=1}^{S}\mathbf{X}_{n,s} \tag{2}$$

$$\tilde{\mathbf{X}}_n = \bar{\mathbf{X}}_n\mathbf{G} \tag{3}$$

$$\mathbf{C} = \frac{1}{N \cdot T - 1}\mathbf{M}\mathbf{M}^{\top}, \mathbf{M} \in \mathbf{R}^{V \times (N \cdot T)} \tag{4}$$

$$\mathbf{C}\mathbf{U} = \mathbf{U}\Lambda \tag{5}$$

$$\mathbf{Y}_n = \mathbf{U}^{\top}\tilde{\mathbf{X}}_n \tag{6}$$

where $\bar{\mathbf{X}}_{n,t}$ refers to the mean activity of trial n in time window t, $\mathbf{X}_{n,s}$ refers to the sample within the time window, $\mathbf{S}$ is the total number of samples in a single window. Gaussian kernel $\mathbf{G}$ is applied for smoothing the averaged time series. All trials are concatenated into a matrix $\mathbf{M}$, with the covariance matrix $\mathbf{C}$ computed based on it. Λ and the columns of $\mathbf{U}$ refer to the diagonal matrix of eigenvalues and the PCA eigenvectors, respectively. $\mathbf{Y}_n$ is the projected trajectory of trial n in PCs space.

Since the principal components (PCs) are linear combinations of multiple voxels' time series, reflecting the activities of combined voxels, while neural modes are spatiotemporal co-activations of multiple neurons, PCs could be regarded as representations of neural modes. As shown in Supplementary Fig.S2, 20 PCs explained most of the variance, so we projected the neural population activities into a 20-dimensional space. In this space, each dimension refers to one PC, representing one neural mode, and neural manifolds refer to the trajectories representing temporal neural dynamics in space.

E. Alignment

To cater to the differences in principal components of different regions and subjects, the low-dimensional representations were projected to a common space for better comparison using canonical correlation analysis (CCA). CCA identifies linear combinations of variables within each view that exhibit maximum correlation with the linear combinations in the other view. For input vectors X and Y, the goal is to find the canonical weights w_x and w_y that maximize the canonical correlation coefficient p.

$$\begin{aligned} p = &\max_{w_x, w_y} w_x^T X Y^T w_y, \\ &s.t. \quad w_x^T X X^T w_x = 1, w_y^T Y Y^T w_y = 1 \end{aligned} \tag{7}$$

where w_x and w_y are canonical weights for X and Y.

This optimization process can be transferred to a generalized eigenvalue problem. If the input views are neural manifolds of different subjects, by multiplying the inputs and obtaining optimal canonical weights, we managed to project the neural manifolds to a common space, which we called alignment.

III. Implementation

A. Evaluation of the Cross-Subject Similarity of Low-Dimensional Neural Manifolds

Cross-subject stability is one of the most important features of low-dimensional latent dynamics of neural population activities [18], [22], proving the universality and effectiveness of

neural-mode-based population dynamics model. To evaluate the cross-subject similarity of our obtained neural manifolds, data from different subjects were paired and all combinations were traversed. CCA was applied to each pair, and the average canonical correlation across all pairs was used to measure cross-subject similarity. That the correlations were calculated only for data from the same ROI and frequency band.

B. Evaluation of Task Dependencies of Low-Dimensional Neural Manifolds

To assess the task relevance of the low-dimensional neural manifolds, we trained two classifiers: a Support Vector Classifier (SVC) and a Random Forest Classifier (RFC). The SVC was trained on data from one subject and tested on data from another, with all subject pairings evaluated. This approach tested both the task specificity and cross-subject consistency of the manifolds. For the RFC, data from all subjects were combined, randomly shuffled, and evaluated using five-fold cross-validation. All classifications were performed at the trial level, with an equal number of trials (13 trials) from motor imagery (MI) and resting states. The mean accuracy across all subject pairs was used to assess SVC performance, while the average across the five folds measured RFC performance. Higher classification accuracy indicates stronger task relevance and greater cross-subject stability of the neural manifolds. Wilcoxon signed-rank test, cohen's d and power calculations were performed to measure the significance and effectiveness of pre- and post-training accuracy differences.

C. Investigation of the Alteration in Neural Manifolds Caused by Stroke Rehabilitation

Since the variances of principal components reflect the information contained in each PC, it is expected to see several neural modes shared high and similar variances in normal neural population activities [18], [22]. Here, by comparing the PC variances before and after BCI training, we explored the training impact on neural manifolds composition.

Further, previous research has identified inter-hemispheric asymmetry as an effective biomarker for stroke rehabilitation [23], [37]. To assess changes in asymmetry during rehabilitation, we calculated the similarity between neural manifolds in regions of interest (ROIs) on both hemispheres. This similarity was measured using canonical correlation, with changes in correlation reflecting alterations in asymmetry.

Lastly, despite the stroke-damaged cortex may achieve functional recovery through functional redistribution [7], it is unclear whether the original neural population dynamics are restored. Thus, the canonical correlation between neural manifolds before and after training was computed to evaluate the changes in neural dynamics. Changes in cross-subject similarity were also estimated by calculating the difference of pre-training and post-training canonical correlation, so as to further investigate the dynamics alteration at a group level.

The above comparisons were conducted on all ROIs and within the theta, alpha, and beta bands, with Wilcoxon signed-rank test to determine significant differences before and after BCI training. Statistical power was calculated to evaluate the reliability of results given the small sample size. To explore the relationship between neural dynamics and motor recovery, we correlated changes in manifold properties—including asymmetry (averaged across canonical components (CC)), and structural differences (measured by Grassmann distance)—with FMA scores. Considering the repetitive and continuous nature of the MI task, to align with the length of resting state data, only the first two seconds of the MI task phase in each trial were taken to compute the low-dimensional neural manifolds for all analyses.

D. Investigation of the Stroke Rehabilitation Impact on Neural Modes

Each neural mode can be mathematically described as a specific linear combination of voxel time series, with its corresponding principal component (PC) vector in the PCA weight matrix serving as its "fingerprint." To assess the impact of BCI training on these neural modes, we computed the cosine similarity between all pre- and post-training fingerprints. For each pre-training mode, the most similar post-training counterpart was identified based on the highest similarity score. We then analyzed changes in similarity and shifts in explained variance rankings to determine how individual neural modes were affected by training. Finally, the average change in explained variance across modes was correlated with FMA scores to evaluate its association with motor recovery.

In addition, while CCA aligns neural manifolds before and after training, it does not directly show how neural modes contribute to each canonical component (CC). To address this, we defined the contribution of each neural mode as the product of its canonical weight and explained variance. By examining how these contributions changed pre- and post-training, we gained insight into the structural modifications of the neural manifold. These analysis were conducted across theta, alpha, and beta bands for all ROIs, with significance analysis (Wilcoxon signed-rank test) and power calculation.

E. Exploration of the Low-Dimensional Latent Dynamics During Resting State

Stroke results in both structural and functional damage, suggesting that changes in neural dynamics are continuous rather than phase-locked. To assess the long-term effects of stroke on neural dynamics, we repeated the mentioned analysis using resting-state data, which also allowed us to explore how motor tasks influence these dynamics. Noting that there were more resting-state trials than MI trials, we selected the first 26 trials for analysis, each lasting 2 seconds.

F. Investigation of the Correlation Between Neural Manifolds and EEG Oscillation

While extensive studies have focused on the characteristics of neural population dynamics as well as its pathological manifestations, the macroscopic representation of these local dynamics needs further exploration. Previous findings have shown a link between neural population dynamics and low- and high-frequency oscillations in local field potentials (LFP) [38]. Inspired by this, we introduced CCA between our obtained neural manifolds and EEG oscillation. Specifically, the EEG oscillation was represented by power spectrum density (PSD) computed using sliding windows of 25 samples

with step of 24 samples on each voxel time series, with the step length selected for aligning the length of PSD series and neural manifolds, and window length selected for maximizing the difference between frequency bands (details of parameter selection mentioned in supplementary material section IV). The PSD series for each voxel was smoothed using the same bin length as the neural manifolds. To match dimensionality, the matrix containing all voxel PSD series underwent PCA too, before conducting CCA. The investigation was carried out on theta, alpha and beta bands and for all ROIs.

G. Validation Based on Acute Stroke Dataset

To reduce the contingency caused by small dataset size, we introduced a public acute stroke dataset (30 subjects, alternating left and right-hand tasks) to further verify our results. The included acute stroke dataset involves MI tasks with a similar paradigm and a wide distribution of NIHSS scores, which reflect varying levels of stroke severity among patients. Considering that the evaluation of stroke rehabilitation also relies on clinical scales, we propose that the pre- and post-rehabilitation brain states of patients can be simulated by dividing patients into high- and low-score groups (differences between groups: $p = 0.0006, cohen's\ d = 4.44, power = 1.00$). To control for potential individual differences, we calculated cross-subject canonical correlations of the neural manifolds for each ROI, which provides confirmation on the preserved cross-subject stability of neural population dynamics in acute stroke patients. This approach allows us to validate most analyses except neural mode tracking on the acute stroke dataset.

IV. Results

A. Stable Low-Dimensional Neural Population Dynamics Exist in the Motor Cortex of Stroke Patients Performing Motor Imagery Tasks

To verify the existence of stable low-dimensional dynamics in the local neural activity of stroke patients during motor imagery tasks, we conducted experiments and recorded whole-brain EEG data following the task paradigm outlined in Fig. 1. Data from the motor imagery phase was selected for further analysis. Fig. 3(b) illustrates the EEG activity projected into voxel space after source localization (trajectories for more subjects can be found in Supplementary Fig.S3 and Fig.S4). The resulting voxel activities display smooth and regular low-dimensional trajectories following windowed averaging, smoothing, and dimensionality reduction, confirming that the simulated neural population activity based on voxel data exhibits meaningful low-dimensional dynamics in time domain.

Furthermore, to demonstrate the stability and task relevance of low-dimensional dynamics, we performed cross-subject alignment and decoding tests on neural manifolds from different subjects. Since our subjects were all right-handed and performed a right-handed grasping MI task, here we focused on the dynamics of the left motor cortex (located in the left precentral gyrus (PreCG,L)) [39], [40]. As shown in Fig. 3(c)., after alignment, the neural manifolds of the PreCG.L from various subjects exhibit a clearer and more similar structure.

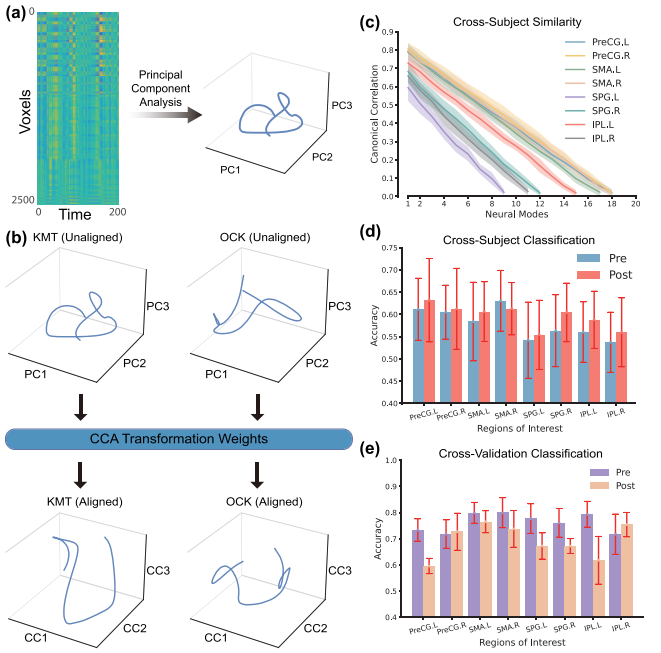

Fig. 3. Obtaining and aligning the low-dimensional dynamics of neural population activities across subjects. **(a)** Schematic diagram of obtaining low-dimensional neural manifolds based on the voxel-time matrix. The number of components for Principal Component Analysis is 20. **(b)** Schematic diagram of aligning neural manifolds across subjects using Canonical Correlation Analysis (CCA). Upper line, 3-dimensional trajectories of neural manifolds before alignment; Lower line, 3-dimensional trajectories of neural manifolds after alignment. **(c)** Canonical correlations across neural manifolds from different subjects. Different colors refer to different ROI. **(d)** Cross-subject classification performance based on neural manifolds. Errorbar, mean ± s.d. Random level, 50%. **(e)** Average of 5-fold cross-validation classification using all subjects. Errorbar, mean ± s.d. Random level, 50%.

Group analysis results indicate that, after alignment, all subject pairs displayed high canonical correlations (Fig. 3(d)). The highest correlations across all ROIs ranged between 0.6 and 0.8, with the precentral gyrus and supplementary motor area maintaining correlations above 0.6 for the top eight canonical components. These findings confirm the structural stability of the low-dimensional neural manifolds across subjects.

We then evaluated classification performance using two approaches: cross-subject decoding with aligned neural manifolds, and five-fold cross-validation with all unaligned manifolds. Results are presented in Fig. 3(d) and (e) as well as Supplementary Fig.S5(b) and Fig.S13. All ROIs showed classification accuracy above the 50% chance level, indicating that the neural manifolds during MI are distinct from those during rest, supporting their task relevance. Notably, while cross-subject accuracy slightly improved after BCI training, accuracy in the cross-validation analysis dropped greatly (PreCG.L, $p = 0.125$, $cohen's\ d = 1.42$, $power = 0.66$), suggesting that BCI training may reduce task-specific distinctiveness of neural population dynamics in the ROIs.

B. Stroke Rehabilitation Leads to Alteration of Neural Population Dynamics

The above results suggest that low-dimensional neural population dynamics manifest potential as a biomarker for tracking stroke rehabilitation. To evaluate the impact of BCI training on these dynamics, we analyzed changes in neural

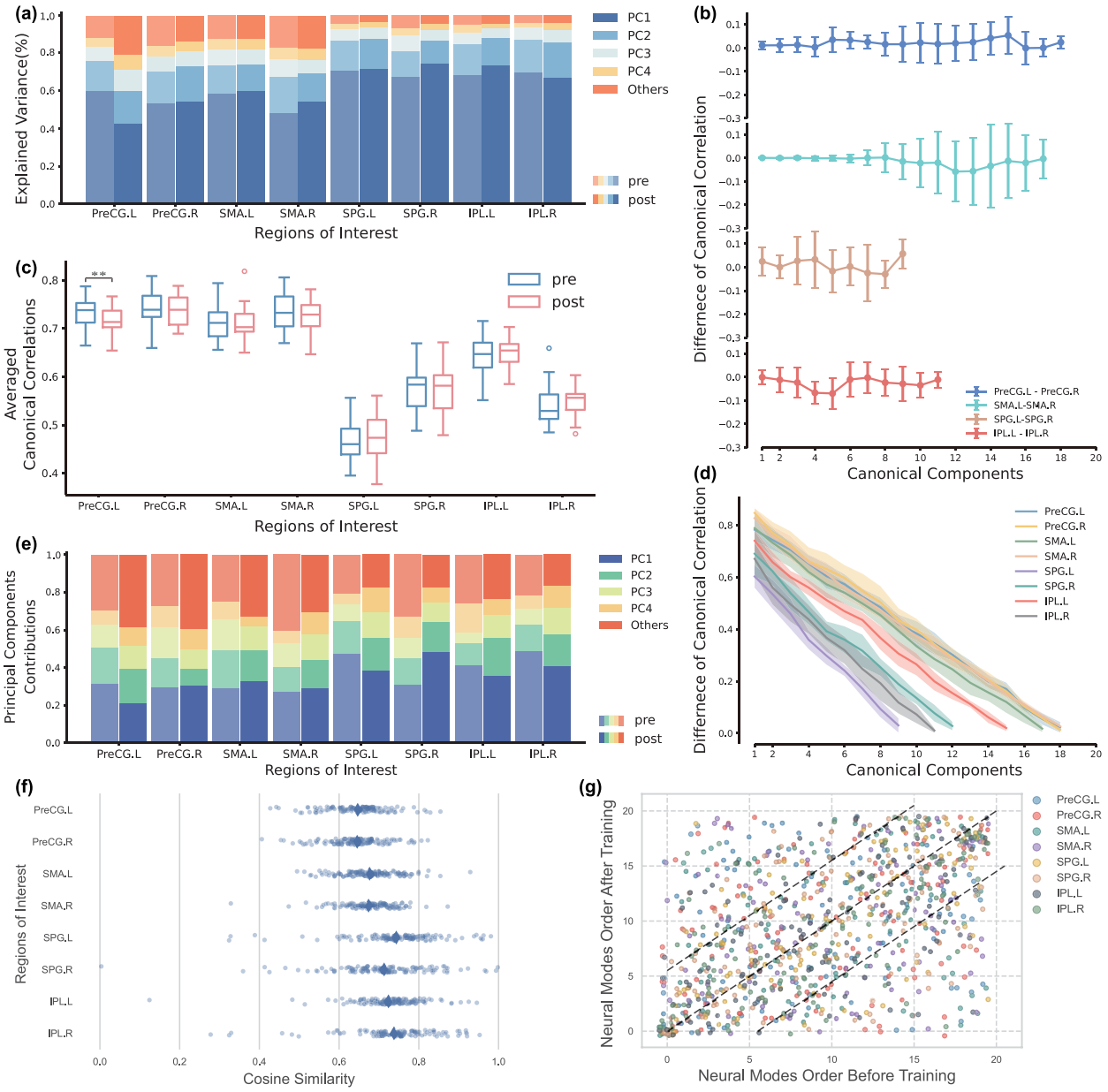

Fig. 4. BCI training induces changes of low-dimensional neural population dynamics in alpha band. **(a)** Explained variances of neural modes before and after BCI training. The top 4 PCs were shown to represent the 4 main neural modes, with others referring to the sum of variances of remaining neural modes. Light colors refer to pre-training variances, while dark colors refer to post-training variances. **(b)** Changes in the asymmetry of corresponding ROIs between the hemispheres before and after training. The difference in interhemispheric canonical correlation was used to assess the asymmetry alteration. The positive difference represents increased asymmetry after training. ErrorBar, mean ± s.d. denotes 0.05 for Wilcoxon signed-rank test. PreCG.L–PreCG.R, $p = 3.75\times10^{-1}$, $cohen's\ d = 0.66$, $power = 0.32$. **(c)** Mean of cross-subject canonical correlations of each ROIs before and after training. The averaged correlation of the top 4 canonical components was used to assess the cross-subject similarity of each pair of subjects. These mean correlations were then averaged across all pairs to get the final values shown on box plot. ** denotes 0.05 for Wilcoxon signed-rank test ($p = 3.51\times10^{-2}$, $cohen's\ d = 0.55$, $power = 0.67$). **(d)** Structural similarity of neural manifolds before and after training. Canonical correlation between pre and post-training neural manifolds was used to assess the similarity. The higher the correlation, the higher the similarity. Different colors refer to different ROIs. **(e)** Contributions of neural modes to canonical component 0 (canonical component (CC) with highest canonical correlation) after alignment between pre- and post-training neural manifolds. The top 4 PCs were shown to represent the 4 main neural modes, with others referring to the sum of contributions of remaining neural modes. Contributions are measured by the product of canonical coefficients and explained variances of PCs. Light colors refer to pre-training contributions, while dark colors refer to post-training contributions. The PCs before and after training only represent the PCs with the top explained variance in the corresponding condition. **(f)** Cosine similarity between corresponding neural modes before and after training. Each semi-transparent dot represents the similarity of a pair of neural modes before and after training, and the solid diamond represents the mean similarity of the brain region. **(g)** Shifts of neural modes order before and after BCI training. The order of neural modes is defined by the ranking of explained variances. Jitters are added to each point to avoid overlapping. The closer the dot is to the diagonal line, the smaller the change in the order of the corresponding neural mode before and after training. Two auxiliary lines are drawn to assist identification of the neural modes with order shift less than 5.

modes, manifold structure, symmetry, and cross-subject stability before and after training. Fig. 4(a) shows the average explained variance of each neural mode in the alpha band across subjects (Similar results were observed in theta and beta band, shown in Supplementary Fig.S5). Changes in neural modes were observed in several ROIs, as reflected by shifts in

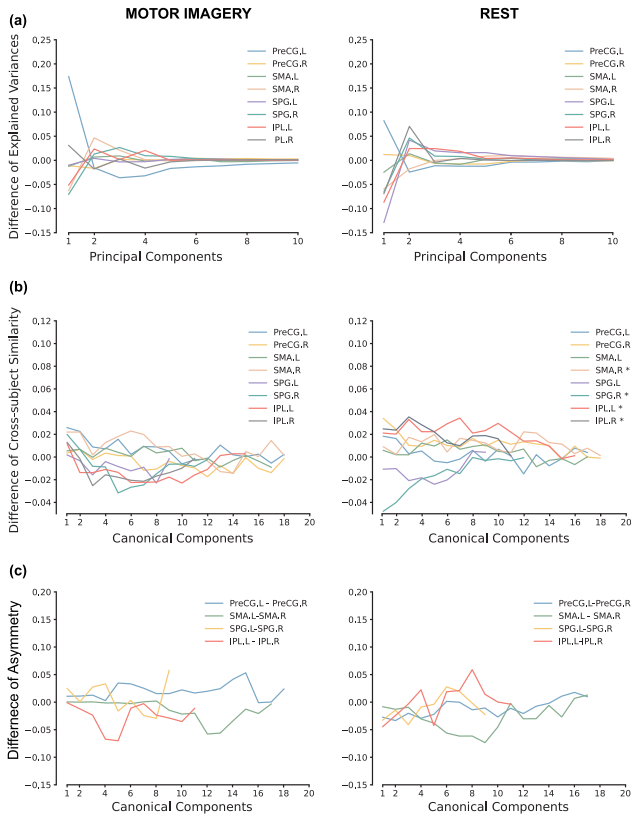

Fig. 5. Comparison between features of low-dimensional neural population dynamics of stroke patients under motor imagery task state and resting state. **(a)** Difference between averaged explained variances across all subjects of the top 10 principal components (neural modes) before and after BCI training. Positive difference refers to decreased variance after BCI training. Left column, results under motor imagery task state; right column, results under resting state. $*$ denotes 0.05 for Wilcoxon signed-rank test. Selected statistical results: PreCG.L, MI, $p = 2.97 \times 10^{-1}$, *cohen's d* $= 0.81$, *power* $= 0.43$; Rest, $p = 6.88 \times 10^{-1}$, *cohen's d* $= 0.20$, *power* $= 0.07$. **(b)** Difference of cross-subject similarity of neural manifolds before and after BCI training. Averaged canonical correlation across all subject pairs was used to assess the similarity. Positive difference suggests decreased cross-subject similarity after BCI training. $*$ denotes 0.05 for Wilcoxon signed-rank test. Selected statistical results: PreCG.L, MI, $p = 4.32 \times 10^{-1}$, *cohen's d* $= 0.23$, *power* $= 0.18$; Rest, $p = 4.12 \times 10^{-1}$, *cohen's d* $= 0.05$, *power* $= 0.06$. **(c)** Difference of asymmetry of corresponding ROIs between the hemispheres before and after training. Averaged interhemispheric canonical correlation across all subjects was used to assess the asymmetry. Positive difference represents increased asymmetry after BCI training. $*$ denotes 0.05 for Wilcoxon signed-rank test. Selected statistical results: PreCG.L–PreCG.R, MI, $p = 3.75 \times 10^{-1}$, *cohen's d* $= 0.66$, *power* $= 0.32$; Rest, $p = 5.78 \times 10^{-1}$, *cohen's d* $= -0.27$, *power* $= 0.09$.

explained variance. Notably, in the left precentral gyrus, the explained variance of the first neural mode exceeded 0.6 before training but dropped to about 0.45 afterward ($p = 1.09 \times 10^{-1}$, $cohen's\ d = 1.18$, $power = 0.74$). Concurrently, the explained variance of the second through fourth neural modes increased. Similar changes were observed in the theta and beta bands (Supplementary Fig.S5). These findings suggest that BCI training promotes stroke rehabilitation by transforming neural population activity in the affected brain region from being dominated by a single neural mode (characterized by excessively high explained variance in the first mode) to a more diverse neural mode distribution (with more balanced explained variances across multiple modes). This shift reflects increased activation and complexity in neural population activity during rehabilitation [7], [21], [41], [42].

We also observed notable changes in hemispheric asymmetry and cross-subject stability. As shown in Fig. 4(b), the canonical correlation between low-dimensional neural manifolds in the left and right motor cortices decreased after BCI training ($p = 3.75 \times 10^{-1}$, $cohen's\ d = 0.66$, $power = 0.32$). In contrast, the opposite trend was seen in the inferior parietal region ($p = 2.19 \times 10^{-1}$, $cohen's\ d = -0.77$, $power = 0.41$). Moreover, cross-subject stability decrease was observed after training, as depicted in Fig. 4(c), where the top four average cross-subject canonical correlations for PreCG.L significantly declined ($p = 3.51 \times 10^{-2}$, $cohen's\ d = 0.55$, $power = 0.67$). Similar results have been observed in *theta* and *beta* bands (Supplementary Fig.S5, Table 3). These findings suggest that BCI training significantly influences neural dynamics, particularly in the motor cortex, where it appears to enhance neural population activity by increasing its diversity, but larger dataset may be needed for further varification.

In terms of structure, only a few ROIs showed significant correlations between changes in neural manifold structure—measured by Grassmann manifold distance—and FMA scores, and no correlation found between asymmetry changes (cross-hemisphere structural similarity) and FMA scores (Supplementary Table 4). Additionally, Fig. 4(d) demonstrates high canonical correlations between neural manifolds before and after BCI training, suggesting that the overall manifold structure remained largely unchanged. However, as shown in Fig.4(e) and Fig.S15, Fig.S16, in motor cortex (especially PreCG.L), post-training neural modes explained less variances (others) provide more contributions to top canonical components compared to pre-training (CC0, PreCG.L, $p = 2.97 \times 10^{-1}$, $cohen's\ d = -0.71$, $power = 0.35$). This indicates that despite the preserved core structure of the manifold, some active neural modes before training may have been suppressed afterward.

Further evidences supporting this interpretation are presented in Fig.4(f), Fig.4(g), and Fig.S14. High similarity (cosine similarity > 0.6; Fig.4(f) and Fig.S14(a)) was observed between neural modes before and after BCI training, confirming that their fundamental structures were maintained. Furthermore, a subset of neural modes manifested substantial shifts in explained variance rankings post-training (order shifts > 5; Fig.4(g)) and Fig.S14(b))), consistent with earlier findings (Fig.4(e)). Changes in neural mode explained variance in multiple brain regions and frequency bands showed strong correlations (> 0.7) and moderate statistical power (> 0.2) with FMA scores (Supplementary Table 4). Together, these results suggest that BCI training enhances motor function primarily by modulating the activation levels of existing neural modes, rather than altering their structures.

C. Task-Specific and Global Effects of BCI Training on Neural Population Dynamics

The classification test revealed differences between neural population dynamics during task and resting states. To further investigate the effects of BCI training on these dynamics under different conditions, we conducted similar analyses using resting-state data. As shown in Fig. 5(c)), Supplementary

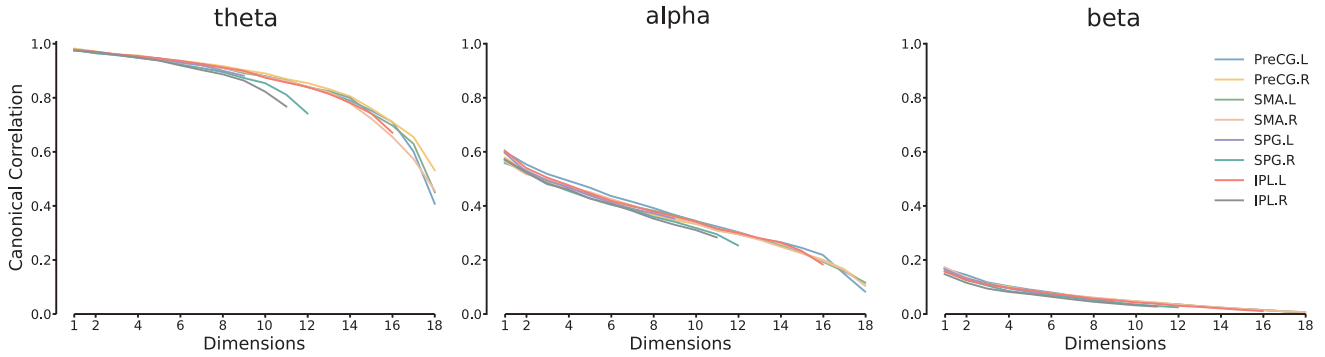

Fig. 6. Correlation between low-dimensional neural population dynamics and EEG oscillations. Averaged Canonical correlation between neural manifolds and low-dimensional representation of power spectrum density time series across all subjects was used to evaluate the correlation. Three frequency bands of EEG, theta, 4-8 Hz; alpha, 8-12 Hz; beta, 12-30 Hz.

Fig.S6 and Table 3, the motor cortex at rest did not exhibit significant changes in hemispheric asymmetry before and after training. Besides, generally lower effect size and power were found in the MI task-related left motor cortex for cross-subject stability in resting-state (Supplementary Table 3). Moreover, while a decrease in explained variance in the resting-state data was observed, the reduction was much smaller than that in the MI task state (Fig. 5(a) and Supplementary Fig.S6). This suggests that BCI-induced changes in motor cortex dynamics are primarily task-related. Nevertheless, we observed significant changes in cross-subject similarity across broader brain regions during rest. Changes in neural mode variances in the resting state also showed higher effect sizes and statistical power, indicating a widespread influence of BCI training on overall brain function. These results suggest that BCI training induces global and sustained changes in brain function and that, in the motor cortex, these changes become more pronounced during the MI task.

D. Low-Dimensional Latent Dynamics Show High Correlation With Low-Frequency Oscillation

To explore the physiological significance of the identified low-dimensional neural manifolds, we conducted a correlation analysis between the manifolds and EEG oscillations. As shown in Fig. 6 and Supplementary Fig.S7, the correlation decreased as frequency increased. Specifically, we found high canonical correlations in the theta band, lower in the alpha band, and lowest in the beta band. These results suggest that the low-dimensional neural manifolds capture information from low-frequency EEG oscillations, indicating they represent the spatiotemporal dynamics of low-frequency neural population activity, supporting previous research findings [38].

E. Acute Stroke Manifests Similar Effects on the Dynamics of Neural Population Activity With Chronic Stroke

To verify whether the stability and task relevance of such low-dimensional dynamics yielded the same results in acute stroke patients, we similarly performed cross-subject alignment and decoding of low-dimensional neural manifolds from different subjects in acute stroke patients. As shown in Supplementary Fig.S8(b) and Fig.S17, after alignment, the low-dimensional neural manifolds from different subjects also exhibited a high similarity in structure when performing the same motor imagery task.

The classification performance of the cross-subject and five-fold cross-validation decoding tests are shown in Supplementary Fig. S9(a) and Fig. S13, all ROIs demonstrated classification accuracy above 60%, significantly higher than random levels, implying that the low-dimensional manifolds of neural dynamics of acute stroke patients, like those of chronic patients, are structurally distinct from the resting state during motor imagery, and similarly demonstrating that these dynamics are task relevance. Similar drops of classification accuracy are also observed between the high and low scores groups of acute stroke dataset.

Unlike chronic stroke patients, in Supplementary Fig.S8(a), it can be observed that the average explained variance of multiple neural modes in the alpha band in acute stroke patients is significantly more complex, and the variance of the first explanation in low score group is generally higher than that in high score group.

Moreover, in the analysis of resting-state data from patients with acute stroke, as shown in Supplementary Fig.S10-11, we also observed significantly greater variability in the explained variance during the MI task state compared to the resting state, as well as significant differences in cross-subject stability. In addition, our results showed that changes in the structure of the neural manifold and interhemispheric asymmetry were significantly correlated with changes in NIHSS scores (Supplementary Table 7). More results based on the acute stroke dataset can be found in Supplementary Fig.S8-12 and Table 6, 7, 8.

V. Discussion

In this study, we implemented BCI-based rehabilitation training for chronic stroke patients and recorded real-time, 64-channel whole-brain EEG during motor imagery tasks before and after the training. Based on the recorded data, we developed a method to derive low-dimensional neural manifolds representing neural population dynamics in specific brain regions and examined how BCI rehabilitation training affected these manifolds. The cross-subject stability, task relevance, and impact of BCI training on neural manifolds and neural modes from both task-state and resting-state EEG were analyzed. To further understand the physiological basis of these manifolds, we also explored their correlation with EEG oscillations. Additionally, to demonstrate that our findings are

not limited to a few individuals, a large public dataset was introduced to validate our findings. The results demonstrate that low-dimensional neural manifolds from EEG data are a valuable tool for characterizing neural population dynamics and show potential as biomarkers for evaluating the effects of BCI training and monitoring stroke rehabilitation progress.

Neural population activity in the motor cortex exhibits stable low-dimensional dynamics during motor tasks [16], [17], [18], [22]. Previous studies have reported that, in both primates and humans, simple movement and motor imagery produce consistent dynamics of neural population activity in the motor cortex across time and subjects [17], [18], [22]. However, these studies typically relied on invasive neural recordings and focused on healthy individuals, with limited application in clinical settings. In this study, we successfully derived low-dimensional neural manifolds of motor cortex neural population activity from whole-brain EEG recordings, which is proven to be stable across subjects and task-related. We observed significant changes in their cross-subject stability, and inter-hemispheric asymmetry, and explained variance of neural modes after BCI training, demonstrating the potential of EEG for exploring local neural population activity. Neural modes and structural alteration of neural manifolds in particular ROIs are also correlated with clinical scores improvement. Our findings support the use of low-dimensional manifolds of neural dynamics as a biomarker for evaluating stroke rehabilitation progress.

Moreover, while the hypothesis of neuronal function remapping and redistribution provides a reasonable explanation for stroke rehabilitation and has been supported by multiple evidences [7], [41], [43], [44], [45], our research provides further clinical evidence on the neural population scale to confirm its validity. We observed a simplification of neural modes in the motor cortex of chronic stroke patients, which diversified following BCI training. In contrast, acute stroke patients showed the opposite pattern. A potential explanation is that during the process of patient transition from acute to chronic stroke stages, natural neuronal function remapping and redistribution may cause the initially disorganized neural modes to stabilize into a single dominant mode. Further rehabilitation then leads to a re-complexification of these neural modes. These findings support the hypothesis of functional remapping and redistribution for stroke rehabilitation. Furthermore, by analyzing changes in neural modes and their contributions to the pre- and post-training aligned canonical components before and after BCI training, we found that training modulates neural population dynamics by activating or suppressing specific neural modes. This observation, along with the reduced task relevance seen in post-training classification performance, suggests a possible interpretation: the dominant neural mode observed before training may represent a pathological, temporary activity pattern that reflects the compensatory overactivation of task-related brain areas after stroke [46], [47]. As rehabilitation progresses, this pattern appears to be replaced by more typical, functionally remapped neural modes, indicating recovery of normal brain function. In addition, by comparing neural manifolds in task and resting states, we noticed that the effects of BCI training were observable even in resting-state data, suggesting that the brain function-repairing process induced by BCI training is global and sustained. Task-related changes were most prominent in the motor cortex, indicating that BCI training primarily restores motor imagery function through motor cortex rehabilitation. This aligns with previous findings [15], [20], [21]. These results suggest that the low-dimensional neural manifolds we identified through EEG recordings can be valuable for further exploring the mechanisms of stroke rehabilitation.

Currently, the physiological basis of stable low-dimensional manifolds of neural dynamics is still not fully understood. Several studies suggested that these dynamics reflect specific neural oscillations [38], [48]. Our findings confirm a high canonical correlation between the low-dimensional neural manifold and EEG theta band oscillations, suggesting that these stable dynamics manifest as low-frequency oscillations at a macro scale. While motor imagery tasks are typically associated with alpha and beta bands oscillation [24], [49], [50], [51], with ERD/ERS in these bands closely linked to the functional deficits resulting from stroke [24], [52], some studies have also identified active dynamics in the theta band in stroke patients during motor imagery [15], [53]. Existing evidences suggest that changes in theta band activity during MI may reflect the reorganization of brain functional networks [54], [55] and adaptive plasticity [56]. Our findings extend this by showing that theta-band changes may indicate the normalization of neural population dynamics. This further demonstrates that changes in theta band activity are likely driven by functional recovery resulted from rehabilitation, rather than the MI task itself.

Last but not least, to validate our findings, we attempted to replicate our results in the chronic stroke dataset on a public dataset of acute stroke patients performing similar motor imagery task [24]. In addition to the differences in explained variance of neural modes, the acute patient results exhibited larger standard deviations, likely reflecting the early-stage functional disruption caused by stroke [19], [21], [43], [57]. With the natural recovery process progresses, such disruption is inhibited by the functional remapping of peripheral neurons [1], [2], [3], [7], which eventually stabilizes the neural modes, resulting in the low standard deviations of chronic patients. This reorganization may be more intense and rapid during the acute phase than in the chronic phase [58], [59], which may explain the stronger associations we observed between clinical scores and structural changes in the acute group. These findings support our earlier hypothesis: stroke rehabilitation first suppresses disorganized activity in the acute phase, leading to simplified patterns, and later modulates specific neural modes in the chronic phase to promote more diverse and functional dynamics.

While the findings outlined above provide a foundational understanding of the low-dimensional dynamics of neural population activity of stroke patients, several issues remain for further exploration. For one thing, the small sample size of our chronic stroke dataset may have limited the statistical power and generalizability of our findings. Although we included data from acute stroke patients and reported effect sizes to mitigate false negatives, the overall analysis remained constrained by the limited dataset. This likely restricted our ability to detect more meaningful patterns and reduced the reliability of our

conclusions, such as limited correlation with clinical scores. Additionally, the lack of diversity in the sample prevented effective control for potential covariates such as gender and lesion side. For example, previous studies suggest that women may experience more severe disability and slower recovery after stroke [60], [61]. Given the underrepresentation of female participants in our dataset, it is possible that observed changes in neural population dynamics are more pronounced and consistent in men, while in women these changes may be subtler or more variable. Future research should involve larger, more diverse populations to validate our methods and strengthen the robustness of the results. For another, both datasets are based on the commonly used number of EEG electrodes (32 or 64) and their setup in clinical settings to facilitate the clinical application. However, this limited electrode coverage may oversimplify neural activity when projected into voxel space, potentially diluting the task-related information and the effect of patient health status in neural manifolds. To this end, future research should involve larger, more diverse populations and high-density EEG or MEG to validate our methods and strengthen the robustness of the results.

VI. Conclusion

In this study, we identified stable low-dimensional neural population dynamics in stroke patients performing motor imagery tasks based on EEG. The uncovered dynamics change globally and sustainably as stroke recovery progresses and can reflect the stroke rehabilitation procedure. Our research offers a novel perspective for understanding the mechanisms of stroke rehabilitation and introduces a potential biomarker for evaluating BCI-based stroke therapies.

References

[1] S. Finger, "Recovery of function: Redundancy and vicariation theories," in *Handbook of Clinical Neurology*, vol. 95. Amsterdam, The Netherlands: Elsevier, 2010, ch. 51, pp. 833–841. [Online]. Available: https://www.ncbi.nlm.nih.gov/pubmed/19892154

[2] S. Finger, P. J. Koehler, and C. Jagella, "The monakow concept of diaschisis: Origins and perspectives," *Arch. Neurol.*, vol. 61, no. 2, pp. 283–288, 2004. [Online]. Available: https://www.ncbi.nlm.nih.gov/pubmed/14967781

[3] T. H. Murphy and D. Corbett, "Plasticity during stroke recovery: From synapse to behaviour," *Nature Rev. Neurosci.*, vol. 10, no. 12, pp. 861–872, Dec. 2009. [Online]. Available: https://www.ncbi.nlm.nih.gov/pubmed/19888284

[4] R. J. Nudo, "Recovery after brain injury: Mechanisms and principles," *Frontiers Hum. Neurosci.*, vol. 7, p. 887, Dec. 2013. [Online]. Available: https://www.ncbi.nlm.nih.gov/pubmed/24399951

[5] J. A. Gallego, M. G. Perich, L. E. Miller, and S. A. Solla, "Neural manifolds for the control of movement," *Neuron*, vol. 94, no. 5, pp. 978–984, Jun. 2017. [Online]. Available: https://www.ncbi.nlm.nih.gov/pubmed/28595054

[6] S. Vyas, M. D. Golub, D. Sussillo, and K. V. Shenoy, "Computation through neural population dynamics," *Annu. Rev. Neurosci.*, vol. 43, no. 1, pp. 249–275, Jul. 2020. [Online]. Available: https://www.ncbi.nlm.nih.gov/pubmed/32640928

[7] B. Campos et al., "Rethinking remapping: Circuit mechanisms of recovery after stroke," *J. Neurosci.*, vol. 43, no. 45, pp. 7489–7500, Nov. 2023. [Online]. Available: https://www.ncbi.nlm.nih.gov/pubmed/37940595

[8] R. Mane, K. K. Ang, and C. Guan, *Brain–Computer Interface for Stroke Rehabilitation*. Singapore: Springer, 2023, pp. 1285–1315, doi: 10.1007/978-981-16-5540-1_33.

[9] M. A. Cervera et al., "Brain-computer interfaces for post-stroke motor rehabilitation: A meta-analysis," *Ann. Clin. Transl. Neurol.*, vol. 5, no. 5, pp. 651–663, May 2018. [Online]. Available: https://www.ncbi.nlm.nih.gov/pubmed/29761128

[10] N. Cheng et al., "Brain-computer interface-based soft robotic glove rehabilitation for stroke," *IEEE Trans. Biomed. Eng.*, vol. 67, no. 12, pp. 3339–3351, Dec. 2020. [Online]. Available: https://www.ncbi.nlm.nih.gov/pubmed/32248089

[11] R. Foong et al., "Assessment of the efficacy of EEG-based MI-BCI with visual feedback and EEG correlates of mental fatigue for upper-limb stroke rehabilitation," *IEEE Trans. Biomed. Eng.*, vol. 67, no. 3, pp. 786–795, Mar. 2020. [Online]. Available: https://www.ncbi.nlm.nih.gov/pubmed/31180829

[12] F. Su and W. Xu, "Enhancing brain plasticity to promote stroke recovery," *Frontiers Neurol.*, vol. 11, Oct. 2020, Art. no. 554089. [Online]. Available: https://www.ncbi.nlm.nih.gov/pubmed/33192987

[13] H.-J. Cheng et al., "Task-related brain functional network reconfigurations relate to motor recovery in chronic subcortical stroke," *Sci. Rep.*, vol. 11, no. 1, p. 8442, Apr. 2021. [Online]. Available: https://www.ncbi.nlm.nih.gov/pubmed/33875691

[14] K. Yuan, X. Wang, C. Chen, C. C. Lau, W. C. Chu, and R. K. Tong, "Interhemispheric functional reorganization and its structural base after BCI-guided upper-limb training in chronic stroke," *IEEE Trans. Neural Syst. Rehabil. Eng.*, vol. 28, no. 11, pp. 2525–2536, Nov. 2020. [Online]. Available: https://www.ncbi.nlm.nih.gov/pubmed/32997632

[15] C. Chen, K. Yuan, X. Wang, A. Khan, W. C.-W. Chu, and R. K.-Y. Tong, "Neural correlates of motor recovery after robot-assisted training in chronic stroke: A multimodal neuroimaging study," *Neural Plasticity*, vol. 2021, pp. 1–12, Jun. 2021. [Online]. Available: https://www.ncbi.nlm.nih.gov/pubmed/34211549

[16] J. A. Gallego, M. G. Perich, S. N. Naufel, C. Ethier, S. A. Solla, and L. E. Miller, "Cortical population activity within a preserved neural manifold underlies multiple motor behaviors," *Nature Commun.*, vol. 9, no. 1, p. 4233, Oct. 2018. [Online]. Available: https://www.ncbi.nlm.nih.gov/pubmed/30315158

[17] J. A. Gallego, M. G. Perich, R. H. Chowdhury, S. A. Solla, and L. E. Miller, "Long-term stability of cortical population dynamics underlying consistent behavior," *Nature Neurosci.*, vol. 23, no. 2, pp. 260–270, Feb. 2020. [Online]. Available: https://www.ncbi.nlm.nih.gov/pubmed/31907438

[18] M. Safaie et al., "Preserved neural dynamics across animals performing similar behaviour," *Nature*, vol. 623, no. 7988, pp. 765–771, Nov. 2023. [Online]. Available: https://www.ncbi.nlm.nih.gov/pubmed/37938772

[19] L. Guo, S. Kondapavulur, S. M. Lemke, S. J. Won, and K. Ganguly, "Coordinated increase of reliable cortical and striatal ensemble activations during recovery after stroke," *Cell Rep.*, vol. 36, no. 2, Jul. 2021, Art. no. 109370. [Online]. Available: https://www.ncbi.nlm.nih.gov/pubmed/34260929

[20] R. J. Nudo, B. M. Wise, F. SiFuentes, and G. W. Milliken, "Neural substrates for the effects of rehabilitative training on motor recovery after ischemic infarct," *Science*, vol. 272, no. 5269, pp. 1791–1794, Jun. 1996. [Online]. Available: https://www.ncbi.nlm.nih.gov/pubmed/8650578

[21] D. S. Ramanathan et al., "Low-frequency cortical activity is a neuromodulatory target that tracks recovery after stroke," *Nature Med.*, vol. 24, no. 8, pp. 1257–1267, Aug. 2018. [Online]. Available: https://www.ncbi.nlm.nih.gov/pubmed/29915259

[22] L. Bashford et al., "Neural subspaces of imagined movements in parietal cortex remain stable over several years in humans," *J. Neural Eng.*, vol. 21, no. 4, Aug. 2024, Art. no. 046059. [Online]. Available: https://www.ncbi.nlm.nih.gov/pubmed/39134021

[23] A. Khan et al., "Changes in electroencephalography complexity and functional magnetic resonance imaging connectivity following robotic hand training in chronic stroke," *Topics Stroke Rehabil.*, vol. 28, no. 4, pp. 276–288, May 2021. [Online]. Available: https://www.ncbi.nlm.nih.gov/pubmed/32799771

[24] H. Liu et al., "An EEG motor imagery dataset for brain computer interface in acute stroke patients," *Sci. Data*, vol. 11, no. 1, p. 131, Jan. 2024. [Online]. Available: https://www.ncbi.nlm.nih.gov/pubmed/38272904

[25] A. Delorme and S. Makeig, "EEGLAB: An open source toolbox for analysis of single-trial EEG dynamics including independent component analysis," *J. Neurosci. Methods*, vol. 134, no. 1, pp. 9–21, Mar. 2004. [Online]. Available: https://www.ncbi.nlm.nih.gov/pubmed/15102499

[26] L. Pion-Tonachini, K. Kreutz-Delgado, and S. Makeig, "ICLabel: An automated electroencephalographic independent component classifier, dataset, and website," *NeuroImage*, vol. 198, pp. 181–197, Sep. 2019. [Online]. Available: https://www.ncbi.nlm.nih.gov/pubmed/31103785

[27] R. Oostenveld, P. Fries, E. Maris, and J.-M. Schoffelen, "FieldTrip: Open source software for advanced analysis of MEG, EEG, and invasive electrophysiological data," *Comput. Intell. Neurosci.*, vol. 2011, no. 1, 2011, Art. no. 156869. [Online]. Available: https://www.ncbi.nlm.nih.gov/pubmed/21253357

[28] R. K. Niazy, C. F. Beckmann, G. D. Iannetti, J. M. Brady, and S. M. Smith, "Removal of FMRI environment artifacts from EEG data using optimal basis sets," *NeuroImage*, vol. 28, no. 3, pp. 720–737, Nov. 2005. [Online]. Available: https://www.ncbi.nlm.nih.gov/pubmed/16150610

[29] Z. Liu, J. A. de Zwart, P. van Gelderen, L.-W. Kuo, and J. H. Duyn, "Statistical feature extraction for artifact removal from concurrent fMRI-EEG recordings," *NeuroImage*, vol. 59, no. 3, pp. 2073–2087, Feb. 2012. [Online]. Available: https://www.ncbi.nlm.nih.gov/pubmed/22036675

[30] J. A. Palmer, K. Kreutz-Delgado, and S. Makeig, "Super-Gaussian mixture source model for ICA," in *Independent Component Analysis and Blind Signal Separation*. Berlin, Germany: Springer, 2006, pp. 854–861.

[31] C.-G. Yan, X.-D. Wang, X.-N. Zuo, and Y.-F. Zang, "DPABI: Data processing & analysis for (resting-state) brain imaging," *Neuroinformatics*, vol. 14, no. 3, pp. 339–351, Jul. 2016. [Online]. Available: https://www.ncbi.nlm.nih.gov/pubmed/27075850

[32] R. Grech et al., "Review on solving the inverse problem in EEG source analysis," *J. NeuroEng. Rehabil.*, vol. 5, no. 1, pp. 1–33, Dec. 2008. [Online]. Available: https://www.ncbi.nlm.nih.gov/pubmed/18990257

[33] R. D. Pascual-Marqui, "Discrete, 3D distributed, linear imaging methods of electric neuronal activity. Part 1: Exact, zero error localization," 2007, *arXiv:0710.3341*.

[34] A. Gramfort, T. Papadopoulo, E. Olivi, and M. Clerc, "OpenMEEG: Opensource software for quasistatic bioelectromagnetics," *Biomed. Eng. OnLine*, vol. 9, no. 1, p. 45, 2010. [Online]. Available: https://www.ncbi.nlm.nih.gov/pubmed/20819204

[35] N. Tzourio-Mazoyer et al., "Automated anatomical labeling of activations in SPM using a macroscopic anatomical parcellation of the MNI MRI single-subject brain," *NeuroImage*, vol. 15, no. 1, pp. 273–289, Jan. 2002. [Online]. Available: https://www.ncbi.nlm.nih.gov/pubmed/11771995

[36] X. Wang et al., "Motor imagery training after stroke increases slow-5 oscillations and functional connectivity in the Ipsilesional inferior parietal lobule," *Neurorehabilitation Neural Repair*, vol. 34, no. 4, pp. 321–332, Apr. 2020. [Online]. Available: https://www.ncbi.nlm.nih.gov/pubmed/32102610

[37] R. Mane et al., "Prognostic and monitory EEG-biomarkers for BCI upper-limb stroke rehabilitation," *IEEE Trans. Neural Syst. Rehabil. Eng.*, vol. 27, no. 8, pp. 1654–1664, Aug. 2019.

[38] C. Gallego-Carracedo, M. G. Perich, R. H. Chowdhury, L. E. Miller, and J. Á. Gallego, "Local field potentials reflect cortical population dynamics in a region-specific and frequency-dependent manner," *eLife*, vol. 11, Aug. 2022, Art. no. e73155. [Online]. Available: https://www.ncbi.nlm.nih.gov/pubmed/35968845

[39] B. M. Dekleva et al., "Motor cortex retains and reorients neural dynamics during motor imagery," *Nature Hum. Behav.*, vol. 8, no. 4, pp. 729–742, Jan. 2024. [Online]. Available: https://www.ncbi.nlm.nih.gov/pubmed/38287177

[40] Z.-Z. Ma et al., "Motor imagery-based brain–computer interface rehabilitation programs enhance upper extremity performance and cortical activation in stroke patients," *J. NeuroEng. Rehabil.*, vol. 21, no. 1, p. 91, May 2024. [Online]. Available: https://www.ncbi.nlm.nih.gov/pubmed/38812014

[41] T. A. Jones, "Motor compensation and its effects on neural reorganization after stroke," *Nature Rev. Neurosci.*, vol. 18, no. 5, pp. 267–280, May 2017. [Online]. Available: https://www.ncbi.nlm.nih.gov/pubmed/28331232

[42] R. P. Rocha et al., "Recovery of neural dynamics criticality in personalized whole-brain models of stroke," *Nature Commun.*, vol. 13, no. 1, p. 3683, Jun. 2022. [Online]. Available: https://www.ncbi.nlm.nih.gov/pubmed/35760787

[43] J. S. Siegel et al., "Disruptions of network connectivity predict impairment in multiple behavioral domains after stroke," *Proc. Nat. Acad. Sci. USA*, vol. 113, no. 30, pp. E4367–E4376, Jul. 2016. [Online]. Available: https://www.ncbi.nlm.nih.gov/pubmed/27402738

[44] M. T. Joy et al., "CCR5 is a therapeutic target for recovery after stroke and traumatic brain injury," *Cell*, vol. 176, no. 5, pp. 1143–1157, Feb. 2019. [Online]. Available: https://www.ncbi.nlm.nih.gov/pubmed/30794775

[45] M. T. Joy and S. T. Carmichael, "Encouraging an excitable brain state: Mechanisms of brain repair in stroke," *Nature Rev. Neurosci.*, vol. 22, no. 1, pp. 38–53, Jan. 2021. [Online]. Available: https://www.ncbi.nlm.nih.gov/pubmed/33184469

[46] C. O. Müller et al., "Brain-movement relationship during upper-limb functional movements in chronic post-stroke patients," *J. NeuroEng. Rehabil.*, vol. 21, no. 1, p. 188, Oct. 2024. [Online]. Available: https://www.ncbi.nlm.nih.gov/pubmed/39438994

[47] A. K. Rehme, S. B. Eickhoff, C. Rottschy, G. R. Fink, and C. Grefkes, "Activation likelihood estimation meta-analysis of motor-related neural activity after stroke," *NeuroImage*, vol. 59, no. 3, pp. 2771–2782, Feb. 2012. [Online]. Available: https://www.ncbi.nlm.nih.gov/pubmed/22023742

[48] S. Dura-Bernal et al., "Multiscale model of primary motor cortex circuits predicts in vivo cell-type-specific, behavioral state-dependent dynamics," *Cell Rep.*, vol. 42, no. 6, Jun. 2023, Art. no. 112574. [Online]. Available: https://www.ncbi.nlm.nih.gov/pubmed/37300831

[49] X. Ma, S. Qiu, and H. He, "Multi-channel EEG recording during motor imagery of different joints from the same limb," *Sci. Data*, vol. 7, no. 1, p. 191, Jun. 2020. [Online]. Available: https://www.ncbi.nlm.nih.gov/pubmed/32561769

[50] M. Kaya, M. K. Binli, E. Ozbay, H. Yanar, and Y. Mishchenko, "A large electroencephalographic motor imagery dataset for electroencephalographic brain computer interfaces," *Sci. Data*, vol. 5, no. 1, Oct. 2018, Art. no. 180211. [Online]. Available: https://www.ncbi.nlm.nih.gov/pubmed/30325349

[51] H. Cho, M. Ahn, S. Ahn, M. Kwon, and S. C. Jun, "EEG datasets for motor imagery brain–computer interface," *GigaScience*, vol. 6, no. 7, pp. 1–8, Jul. 2017. [Online]. Available: https://www.ncbi.nlm.nih.gov/pubmed/28472337

[52] G. Pfurtscheller and F. H. L. da Silva, "Event-related EEG/MEG synchronization and desynchronization: Basic principles," *Clin. Neurophysiol.*, vol. 110, no. 11, pp. 1842–1857, Nov. 1999. [Online]. Available: https://www.ncbi.nlm.nih.gov/pubmed/10576479

[53] J. J. Zhang, Z. Bai, and K. N. K. Fong, "Resting-state cortical electroencephalogram rhythms and network in patients after chronic stroke," *J. NeuroEng. Rehabil.*, vol. 21, no. 1, p. 32, Feb. 2024. [Online]. Available: https://www.ncbi.nlm.nih.gov/pubmed/38424592

[54] M. Lee, Y.-H. Kim, and S.-W. Lee, "Motor impairment in stroke patients is associated with network properties during consecutive motor imagery," *IEEE Trans. Biomed. Eng.*, vol. 69, no. 8, pp. 2604–2615, Aug. 2022. [Online]. Available: https://www.ncbi.nlm.nih.gov/pubmed/35171761

[55] Y. Fu, Z. Zhou, A. Gong, Q. Qian, L. Su, and L. Zhao, "Decoding of motor coordination imagery involving the lower limbs by the EEG-based brain network," *Comput. Intell. Neurosci.*, vol. 2021, no. 1, Jan. 2021, Art. no. 5565824. [Online]. Available: https://www.ncbi.nlm.nih.gov/pubmed/34257636

[56] N. Rustamov, J. Humphries, A. Carter, and E. C. Leuthardt, "Theta–gamma coupling as a cortical biomarker of brain–computer interface-mediated motor recovery in chronic stroke," *Brain Commun.*, vol. 4, no. 3, p. 136, May 2022. [Online]. Available: https://www.ncbi.nlm.nih.gov/pubmed/35702730

[57] J. Wu, R. Srinivasan, E. B. Quinlan, A. Solodkin, S. L. Small, and S. C. Cramer, "Utility of EEG measures of brain function in patients with acute stroke," *J. Neurophysiology*, vol. 115, no. 5, pp. 2399–2405, May 2016. [Online]. Available: https://www.ncbi.nlm.nih.gov/pubmed/26936984

[58] C. Grefkes and G. R. Fink, "Recovery from stroke: Current concepts and future perspectives," *Neurol. Res. Pract.*, vol. 2, no. 1, p. 17, Dec. 2020. [Online]. Available: https://www.ncbi.nlm.nih.gov/pubmed/33324923

[59] Y. Xia et al., "Dynamic structural and functional reorganizations following motor stroke," *Med. Sci. Monitor*, vol. 27, Jan. 2021, Art. no. 929092. [Online]. Available: https://www.ncbi.nlm.nih.gov/pubmed/33707406

[60] C. Carcel et al., "Sex differences in treatment and outcome after stroke: Pooled analysis including 19,000 participants," *Neurology*, vol. 93, no. 24, pp. e2170–e2180, 2019. [Online]. Available: https://www.ncbi.nlm.nih.gov/pubmed/31719135

[61] S. Paolucci et al., "Is sex a prognostic factor in stroke rehabilitation? A matched comparison," *Stroke*, vol. 37, no. 12, pp. 2989–2994, 2006. [Online]. Available: https://www.ncbi.nlm.nih.gov/pubmed/17082475